Measurements of the third- and fifth-order optical nonlinearities of water at 532 and 1064 nm using the D4σ method

Côme Schnebelin, Christophe Cassagne, Cid de Araújo, Georges Boudebs

Measurements of the third- and fifth-order optical nonlinearities of water at 532 and 1064 nm using the D4σ method

Côme Schnebelin,[1] Christophe Cassagne,[1] Cid B. de Araújo,[2] and Georges Boudebs[1,*]

[1]*LUNAM Université, Université d'Angers, LPhiA, Laboratoire de Photoniques d'Angers, EA 4464, 49045 Angers Cedex 01, France*

[2]*Departamento de Física, Universidade Federal de Pernambuco, 50670-901 Recife, Pernambuco, Brazil*

**Corresponding author: georges.boudebs@univ-angers.fr*

Received June 19, 2014; revised July 16, 2014; accepted July 16, 2014;
posted July 17, 2014 (Doc. ID 214367); published August 20, 2014

The nonlinear response of liquid water was investigated at 1064 and 532 nm using a Nd:YAG laser delivering pulses of 17 ps and its second harmonic. The experiments were performed using the D4σ method combined with the *Z*-scan technique. Nonlinear refractive indices of third- and fifth-order were determined, as well as the three-photon absorption coefficient, for both wavelengths. A good agreement was found between theory and experiment. © 2014 Optical Society of America

OCIS codes: (160.4330) Nonlinear optical materials; (190.4420) Nonlinear optics, transverse effects in; (190.4180) Multiphoton processes; (260.5950) Self-focusing; (050.5080) Phase shift.
http://dx.doi.org/10.1364/OL.39.005046

High-order optical nonlinearities (HON) in gases and condensed matter are still deserving investigations from the fundamental point of view [1–4] as well as because of their important role in phenomena such as soliton formation [5,6], filamentation in gases [7], supercontinuum generation [8], and other transverse nonlinear (NL) effects [9–11]. In particular, in the regime of high laser intensity, the investigation of self-focusing of light in transparent materials is important to understand light filamentation in condensed matter that occur without destruction of the material being investigated. This was argued for solids [12] and more recently it was demonstrated for liquid CS_2 [13], where it was found that the effective NL optical parameters show saturation of the Kerr effect and were responsible for filamentation. However, with respect to water, the contribution of HON for the prefilamentation regime was not demonstrated. Although previous publications were dedicated to the study of water [14–16], the influence of the fifth-order nonlinearity in the picosecond regime was not recognized.

Therefore, the aim of this paper is to provide an insight into relevant NL parameters associated to self-focusing using high laser intensities in the case of water. It is shown that for understanding the water behavior near filamentation it is important to consider the influence of the fifth-order nonlinearity that may contributes to focus or defocus the light and/or acts as an intensity limiting mechanism. The experiments were performed using the D4σ method [17] that allows accurate measurements especially in presence of NL absorption. Measurements of the fifth-order refractive index and three-photon absorption (3PA) coefficient of water are reported for the first time at 532 and 1064 nm.

We consider a beam propagating along the z' axis in a sample exhibiting linear absorption [coefficient α (m^{-1})], two-photon absorption (2PA) [coefficient β (m/W)], 3PA [coefficient γ (m^3/W^2)], Kerr effect [third-order NL refractive index n_2 (m^2/W), and fifth-order NL refractive index n_4 (m^4/W^2)]. Under the slowly varying envelope and thin sample approximations, the optical intensity I (GW/cm^2) and the phase φ satisfy the equations

$$\frac{dI}{dz'} = -\alpha I - \beta I^2 - \gamma I^3, \tag{1}$$

$$\frac{d\varphi}{dz'} = k(n_2 I + n_4 I^2), \tag{2}$$

where $k = 2\pi/\lambda$ is the modulus of the wave vector and λ is the wavelength. Equations (1) and (2) govern the evolution of the intensity and the NL phase-shift as a function of the propagation distance z' in the medium, when considering the sample thickness L smaller than the confocal parameter of the incident focused beam.

Equations (1) and (2) can be solved performing a numerical inversion by means of Newton's method and the solutions were obtained even when n_2, n_4, 2PA, and 3PA are non-null. This analysis allowed us to determine the third- and fifth-order susceptibilities in the case of CS_2 [18]. In the particular case of water, with $\alpha = \beta = 0$ and taking into account the boundary conditions $[I(z' = 0) = I_0; I(z' = L) = I_L]$, the solutions are given by

$$\Delta\varphi = \frac{-k}{\gamma}\left[n_2 \frac{I_L - I_0}{I_L I_0} + n_4 \ln\left(\frac{I_L}{I_0}\right)\right], \tag{3}$$

$$I_L = I_0(1 + 2\gamma I_0^2 L)^{-1/2}. \tag{4}$$

The experimental setup used to implement the D4σ method [17] is sketched in Fig. 1. The sample was supported on a translation stage and moved along the beam direction (z axis) in the focus region. The process was controlled by a computer allowing, for each step of the motor, to open a shutter (not shown in the figure) and to acquire an image of the output pulse recorded by the CCD camera. A second arm was used to monitor

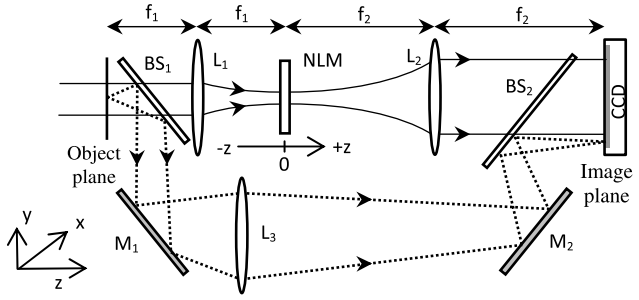

Fig. 1. $4f$ imaging system. The sample is scanned along the beam direction around the focal plane ($z = 0$). The labels refer to: lenses (L_1, L_2, and L_3), beam splitters (BS_1 and BS_2), and mirrors (M_1 and M_2).

the energy fluctuation of the incident laser beam. The imaging system can be described on the basis of Fourier-optics [19]). The object used to characterize the NL medium is placed before lens L_1, where any beam profile can be used. We used a circular object (top-hat beam) with an optimized radius for each wavelength to obtain a Rayleigh range larger than the sample thickness and smaller than the motor scanning length. The induced instantaneous phase-shift originates changes in the transmitted beam waist in the image plane while moving the sample in the focal region, and this allows determination of the phase-shift due to NL refraction. Note that lens L_2 contributes to produce the Fourier-transform of the field at the exit surface of the sample, which is physically similar to the far-field diffraction pattern obtained with the original Z-scan method [20]. Moreover, this lens produces an image of the object plane that allows us to characterize accurately the profile of the beam at the entry which is a very important parameter to characterize the optical object precisely.

The numerical procedure followed in the Fourier domain has the advantage to reduce the computing time. Using the optical transfer function related to the free-space propagation over a finite distance, and considering the phase transformations due to lenses L_1 and L_2, we can simulate the propagation of the beam from the object to the image plane taking into account the NL medium positioned at each motor step of the Z-scan procedure. The transmittance of the NL medium is considered by means of the appropriate functions derived from Eqs. (3) and (4). Finally, fits of the Z-scan profiles provide the NL parameters of the medium by comparing numerical and experimental data. Notice that, in the D4σ experiment, a top-hat beam was used and the second moment of $I(x, y)$ is measured; the method gives four times the standard deviation of the intensity distribution [17], whereas the Z-scan method is based on transmission measurement.

In the measurements, a 2 mm thick cell filled with water was used (Fluka ref. 95305 from Sigma–Aldrich) excited by a Nd:YAG laser delivering linearly polarized pulses at $\lambda = 1.064$ μm (17 ps FWHM) and 532 nm (12 ps FWHM) with a repetition rate smaller than 1 Hz. For detection we used a cooled (–30°C) 1000 × 1018 pixels CCD camera with a fixed linear gain. Each pixel 12 μm × 12 μm shows 4095 gray levels. The input intensity I_0 could be varied by means of a half-wave plate and a Glan prism. Two sets of acquisitions are performed. The first one is in the NL regime and the second one in the linear regime (by reducing the incident energy of the laser under the detection limit of the joulemeter). The linear acquisitions are necessary to remove the diffraction, diffusion, and/or imperfection effects due to sample inhomogeneities from the NL measurements. Moreover, an image of the entry plane of the $4f$ system allows characterization of the object that will be considered in the simulation. The sensitivity of the setup depends on parameters such as the object profile and the wavelength, and is calculated for each set of acquisitions taking into account the real beam profile. This procedure allows high accuracy measurements, even for relatively large absorption and phase-shift, when the signal is no longer linear with the beam waist relative variation (for details on the numerical procedure see [17,21]). It is important to note that absolute measurements were performed [22], thus avoiding an intensity calibration based on a reference material. The main source of uncertainty comes from the absolute measurement of the laser pulse energy; the accuracy of the joulemeter is about 10%. To take into account the contributions of the cells' walls and water in the focus, the total phase induced by the incident light is written as $\Delta\varphi_{\text{tot}} = \Delta\varphi_c + \Delta\varphi_w$, from which one can estimate the effective NL index of water: $n_{2w} = [(\lambda\Delta\varphi_{\text{tot}}/2\pi I_0) - n_{2c}L_c]/L_w$, where c stands for cell and w for water. As will be shown, the absorption in the quartz cell is negligible according to the observed total NL absorption of water alone.

Figure 2(a) shows the beam waist relative variation versus z for experiments with a 2.46 mm thick quartz cell filled with 2 mm of water, for $I_0 = 880$ GW/cm^2 at $\lambda = 1064$ nm. The black filled circles are obtained with the cell containing water and the red non-filled circles represent the data for the empty cell. The red solid line is the fitting for silica alone, giving: $n_2 = (4.4 \pm 0.9) \times 10^{-21}$ m^2/W, in agreement with [22], and the black dashed line is obtained with the determined parameters for water: $n_2 = (1.0 \pm 0.2) \times 10^{-22}$ m^2/W, $n_4 = (1.1 \pm 0.3) \times 10^{-36}$ m^4/W^2, and $\gamma = (3.6 \pm 0.9) \times 10^{-30}$ m^3/W^2. The γ value was obtained from Fig. 2(b), which shows the open-aperture Z-scan normalized transmittance. The black dashed line is the simulation obtained with the γ value for water (filled circles). Note the negligible NL absorption of quartz alone (red empty circles).

Figure 3(a) shows the beam waist relative variation versus z for the same cell with $I_0 = 290$ GW/cm^2 at $\lambda = 532$ nm. The black circles were obtained with water inside the cell and the red empty circles represent the data for the empty cell. The solid red line is the fitting, giving $n_2 = (8.1 \pm 1.6) \times 10^{-21}$ m^2/W, which is in agreement with [22] for the empty cell. The dashed line is obtained with the measured parameters $n_2 = (9.6 \pm 2.4) \times 10^{-21}$ m^2/W, $n_4 = (7.4 \pm 2.2) \times 10^{-36}$ m^4/W^2, and $\gamma = (4.0 \pm 1.1) \times 10^{-29}$ m^3/W^2. The γ value was obtained from the open-aperture Z-scan normalized transmittance shown in Fig. 3(b). The dashed line is the simulation obtained with the previous value of γ for water (filled circles). The NL absorption of quartz alone (red empty circles) is very small in comparison with the NL absorption of water. Because the thin sample approximation was used the values for the NL parameters at high intensities could be over-estimated due to the self-focusing

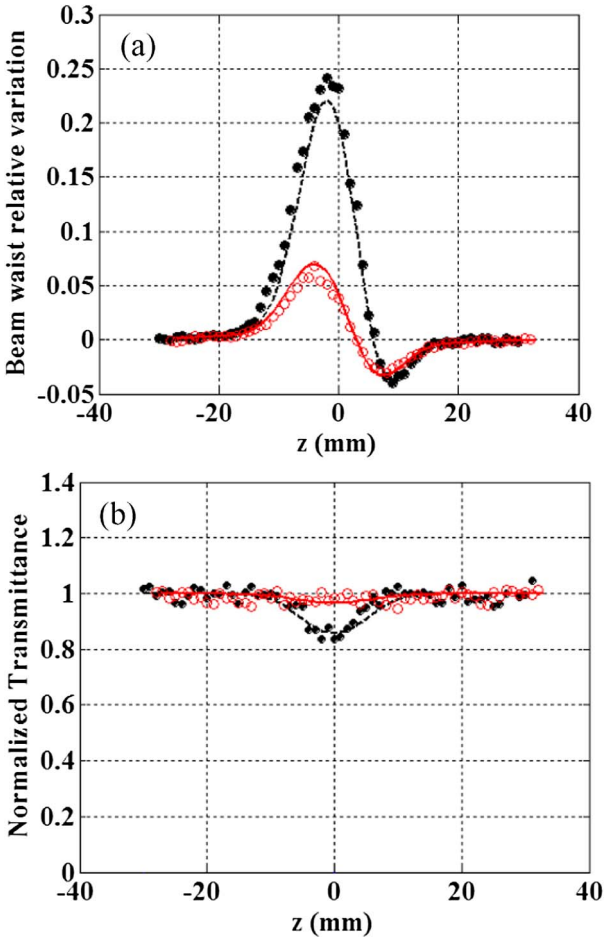

Fig. 2. 2.46 mm thick quartz cell filled with 2 mm water measured at $\lambda = 1064$ nm with $I_0 = 880$ GW/cm^2. The black circles were obtained with water inside the cell; the empty red circles were obtained with the cell alone. (a) Beam waist relative variation versus z; (b) open-aperture normalized Z-scan transmittance. Dashed and solid lines represent the fittings.

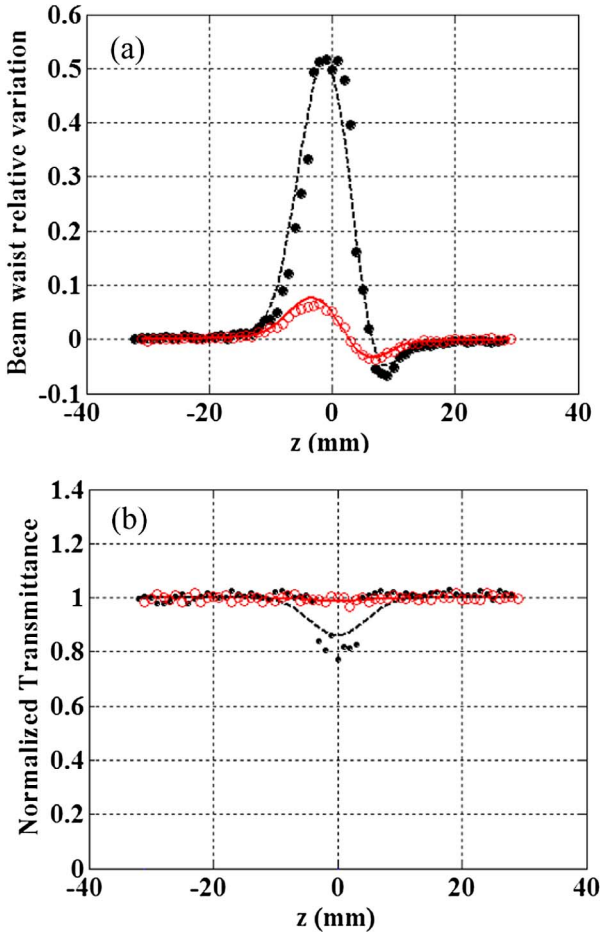

Fig. 3. 2.46 mm thick quartz cell filled with 2 mm water measured at $\lambda = 532$ nm with $I_0 = 290$ GW/cm^2. The filled circles are data obtained with the cell containing water; the red empty circles represent data obtained with the cell alone. (a) Beam waist relative variation versus z; (b) open-aperture normalized Z-scan transmittance. Dashed and solid lines represent the fittings.

increasing the effective irradiance while the beam propagates inside the sample. Estimation at 532 nm using 300 GW/cm^2 increased by 26% the output intensity after 2 mm propagation in water, leading to about 13% underestimated value of the mean irradiance along the sample.

Figure 4 summarizes the results for the effective NL refractive indices, $n_{2\text{eff}}$, versus the laser intensity. The data for the empty quartz cell are represented by black squares ($\lambda = 532$ nm) and red circles ($\lambda = 1064$ nm), giving the mean values of n_2 for both wavelengths used previously, while the measurements for water are represented by green stars ($\lambda = 532$ nm) and blue triangles ($\lambda = 1064$ nm). Notice that while the data for the empty cell remains constant for increasing laser intensities, $n_{2\text{eff}}$ for water at both wavelengths increases with the intensity. This dependence indicates that high-order nonlinearities are contributing for the results and the linear behavior with the intensity indicates that the contribution of fifth-order is important even for relatively low NL phase shift ($<\pi$). Therefore, the straight lines drawn in the figure represent the fitting using $n_{2\text{eff}} = n_2 + n_4 I$, giving $n_2 = (1.0 \pm 0.2) \times 10^{-22}$ m^2/W and $n_4 = (1.1 \pm 0.3) \times 10^{-36}$ m^4/W^2 for $\lambda = 1064$ nm. For $\lambda = 532$ nm we obtained $n_2 = (9.6 \pm 2.4) \times 10^{-21}$ m^2/W and $n_4 = (7.4 \pm 2.2) \times 10^{-36}$ m^4/W^2.

The results reported can be analyzed considering that the NL response of water excited by high laser intensities could be due to self-focusing, multiphoton absorption (MPA), and laser induced breakdown. In principle, these three mechanisms compete, with the dominant parameters being the laser intensity and wavelength used [15]. According to [15] for high laser intensities the amount of ionized molecules would be large and the plasma that is formed would contributes to $n_{2\text{eff}}$. Then, if the contribution of ionized molecules were important, the slope of the straight line would change for larger laser intensities due to the plasma negative nonlinearity. However, the positive slopes observed for both wavelengths indicate that the NL response is dominated by MPA in the range of intensities used. This conclusion is corroborated by the fit of the open-aperture Z-scan experiments shown in Figs. 2 and 3, where the curves based on the 3PA process fit reasonably to the experimental data; although, a small disagreement indicates that higher-order MPA might be contributing, too. We recall that two-photon induced dissociation of water was

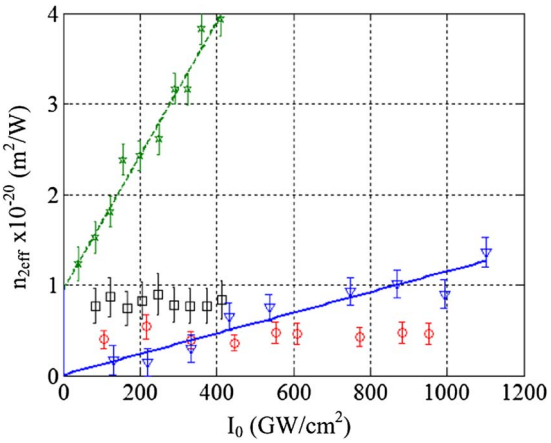

Fig. 4. Effective n_2 versus the incident intensity. The data for the empty cell are the squares (circles) at 532 nm (1064 nm). The measured values for water alone are the green stars (blue triangles) at 532 nm (1064 nm). The straight lines represent the linear fitting at 1064 and 532 nm.

observed using a laser at 266 nm [23]. The energy of the absorbed photons corresponds to the energy of four photons being absorbed in the present experiment. Finally, we mention that the behavior of $n_{2\text{eff}}$ is analogous to the behavior reported for CS_2 [13]. Unfortunately we could not perform experiments at higher intensities due to laser power limitations and probable saturation of the NL refractive index could not be observed. However, filamentation was observed using a 5 cm long cell with the available powers.

In summary, we reported here the use of the D4σ method for measurements of the third- and fifth-order nonlinearity of liquid water at room temperature. The results indicate that, at intermediate intensities defining the pre-filamentation, the NL response of water is dominated by the non-ionized molecules, and can be described by a linear variation of the effective NL refractive index versus the laser intensity. The density of ionized molecules, in the range of intensities used here, does not saturate the NL response of water.

We acknowledge financial support from the "Région Pays de la Loire" for the senior foreign research chair contracted to C. B. de Araújo. We also acknowledge E. W. Van Stryland for a critical reading of the manuscript.

References

1. K. Dolgaleva, H. Shin, and R. W. Boyd, Phys. Rev. Lett. **103**, 113902 (2009).
2. C. Brée, A. Demircan, and G. Steinmeyer, Phys. Rev. Lett. **106**, 183902 (2011).
3. N. J. Dawson and J. H. Andrews, J. Phys. B **45**, 035401 (2012).
4. B. B. Zhou, A. Chong, F. W. Wise, and M. Bache, Phys. Rev. Lett. **109**, 043902 (2012).
5. E. D'Asaro, S. Heidari-Bateni, A. Pasquazi, G. Assanto, J. Gonzalo, J. Solis, and C. N. Afonso, Opt. Express **17**, 17150 (2009).
6. E. L. Falcão-Filho, C. B. de Araújo, G. Boudebs, H. Leblond, and V. Skarka, Phys. Rev. Lett. **110**, 013901 (2013).
7. M. Kolesik, E. M. Wright, and J. V. Moloney, Opt. Lett. **35**, 2550 (2010).
8. J. M. Dudley and G. Genty, Phys. Today **66**(7), 29 (2013).
9. Z. Chen, M. Segev, and D. N. Christodoulides, Rep. Prog. Phys. **75**, 086401 (2012).
10. W. Zhu, Y. He, B. A. Malomed, and D. Mihalache, J. Opt. Soc. Am. B **31**, A1 (2014).
11. A. S. Reyna and C. B. de Araújo, Phys. Rev. A **89**, 063803 (2014).
12. B. Borchers, C. Brée, S. Birkholz, A. Demircan, and G. Steinmeyer, Opt. Lett. **37**, 1541 (2012).
13. V. Besse, H. Leblond, and G. Boudebs, Phys. Rev. A **89**, 043840 (2014).
14. C. A. Sacchi, J. Opt. Soc. Am. B **8**, 337 (1991).
15. Q. Feng, J. V. Moloney, A. C. Newell, and E. M. Wright, Opt. Lett. **20**, 1958 (1995).
16. A. Dubietis, A. Couairon, E. Kučinskas, G. Tamošauskas, E. Gaižauskas, D. Faccio, and P. di Trapani, Appl. Phys. B **84**, 439 (2006).
17. G. Boudebs, V. Besse, C. Cassagne, H. Leblond, and C. B. de Araújo, Opt. Lett. **38**, 2206 (2013).
18. V. Besse, G. Boudebs, and H. Leblond, "Determination of the third- and fifth-order optical nonlinearities: the general case," Appl. Phys. B, doi: 10.1007/s00340-014-5777-2 (2014).
19. K. Fedus and G. Boudebs, Opt. Commun. **292**, 140 (2013).
20. M. Sheik-Bahae, A. A. Said, T.-H. Wei, D. Hagan, and E. W. Van Stryland, IEEE J. Quantum Electron. **26**, 760 (1990).
21. G. Boudebs, K. Fedus, C. Cassagne, and H. Leblond, Appl. Phys. Lett. **93**, 021118 (2008).
22. G. Boudebs and K. Fedus, J. Appl. Phys. **105**, 103106 (2009).
23. J. Underwood and C. Wittig, Chem. Phys. Lett. **386**, 190 (2004).